Surface Science 290 (1993) 179–194
North-Holland

surface science

Molecular dynamics simulations of the basal planes of Ni and Cu using Finnis–Sinclair potentials

D.D. Koleske [1] and S.J. Sibener [2]

Department of Chemistry and The James Franck Institute, University of Chicago, 5640 South Ellis Avenue, Chicago, IL 60637, USA

Received 7 December 1992; accepted for publication 26 January 1993

Using MD simulations, we have calculated the surface phonon spectral density functions for the (100), (110), and (111) surfaces of Ni and Cu using Finnis–Sinclair (FS) potentials. These simulated phonon spectral densities are compared to the experimental inelastic helium atom scattering and HREELS data which are available for the three basal faces of Ni and Cu. We find that the overall shape of the calculated surface and second layer phonon spectral densities qualitatively reproduce those obtained from force constant fits, i.e. lattice dynamical modelling, of the experimental phonon dispersion data. Good agreement is also found between the calculated and experimental geometric separations between the surface and second layer for a given interface. However, on all surfaces the phonon frequencies calculated with Finnis–Sinclair potentials are lower than the experimentally measured values. The best agreement between our calculated results and the experimentally measured phonon frequencies was for the (100) and (110) surfaces, while the poorest agreement was on the (111) surfaces. From this we conclude that Finnis–Sinclair model potentials derived from bulk properties systematically underestimate the many body binding potential at the surface. This underestimation of the many body binding term is also manifested in the magnitude of the calculated surface stress. Our results indicate that the Finnis–Sinclair model potentials are quite adequate for a good qualitative and semi-quantitative description of the bonding changes at the surfaces of Ni and Cu.

1. Introduction

The many successes of density functional derived model potentials have been recently demonstrated [1–15]. Carlsson has called these pair functional model potentials [1] and they include the embedded atom method (EAM) [2–6], effective medium theory (EMT) [7–10], "glue" models [11–13], and Finnis–Sinclair (FS) models [14,15]. These various model potentials have been used to predict changes in surface bonding, possible reconstructions, changes in interlayer spacings, and changes in surface force fields. The emergence of these non-central potential models is essential for both predicting surface phenomena and for developing simple physical models of the changes that occur in bonding at surfaces.

All of these methods make the assumption that the total energy of the solid can be described as a sum of a repulsive two-body pair potential and a many body cohesive potential [1]. The cohesive potential is a functional of the local electron density, which can be assumed to be a sum of the individual atomic electron densities such as in the EAM [2] and FS [14] potentials. The functional form of the cohesive potentials are usually chosen so that potential correctly reproduces as many bulk properties of the metal as possible [1]. For example, the EAM generates this attractive many body binding potential by fitting to bulk properties, such as the bulk modulus, lattice cohesive energy, and defect creation energies [2]. On the other hand, the EMT method attempts to derive appropriate functions to describe the various energy terms, such as electron–ion and electron–electron correlation terms which

[1] Current address: IBM, T.J. Watson Research Center, P.O. Box 218, Yorktown Heights, NY 10598.

[2] 1992/93 Visiting Fellow, Joint Institute for Laboratory Astrophysics, University of Colorado, Boulder, CO 80309-0440, USA.

when summed together describe the energy of the solid [7].

The popularity of these model potentials stems from the wide array of surface properties which can be calculated when they are used [1]. These methods have been used to calculate the surface energy, surface stress, surface reconstruction energy, and interlayer contraction between the surface and second layer for some of the noble (Cu, Ag, and Au) and group VIII-B metals (Ni, Pd, and Pt) [1–3,14]. One property these methods have predicted correctly is the reduction in the first-to-second interlayer spacing as compared to bulk values. The reason for this, as explained by Carlsson, involves electronic charge redistribution at the surface to lower the kinetic energy of the surface electrons, i.e. a "smoothing" of the surface electronic states [1]. As a result of this smoothing, the density of electronic states at the surface is compressed in energy which increases the amount of cohesive bonding at the surface [1].

EAM and EMT potentials have qualitatively and somewhat quantitatively reproduced the surface phonon dispersion curves for a number of metal surfaces [5,6,8–10,16,17]. In particular, Nelson et al. [6] using the EAM have explained the inconsistency between the two different force constant models derived to explain the helium atom scattering (HAS) [18] and high resolution electron energy loss spectroscopy (HREELS) [19] measured surface phonon dispersions on Cu(111). The origin of this inconsistency is an avoided crossing between the first and second layer longitudinal models with the z-polarized second layer mode. In addition to calculating lattice dynamics at low temperatures, these potentials have been used in molecular dynamics simulations to calculate the temperature dependence of surface phonon spectral densities [10]. Temperature dependent surface phonon spectral densities on Cu(110) have been calculated using EMT potentials [10]. Here the rate at which the phonon frequency decreased and the phonon linewidth increased agreed well with the experimental results obtained from HREELS [20].

The surface vibrational dynamics of the basal planes of both Ni and Cu have been extensively studied experimentally [19,21–29]. Some of the pioneering HREELS experiments measured the surface phonon dispersion of Ni(100) [21,22], and were followed by further work on Ni(110) [23], and Ni(111) [24]. The surface phonon dispersion curves have also been measured for Cu(100) [25,26], Cu(110) [27,28], and Cu(111) [19,29]. In the Ni papers it is argued that the vibrational dynamics of bulk Ni can be described using a single force constant model, therefore single force constant models might be adequate to describe the surface phonon dispersion curves on the three basal surfaces. However, if a single force constant model is extended to the surface, it predicts Rayleigh wave frequencies that are too low in energy. This discrepancy can be accounted for by stiffening the force constants between the first and second layer. A more sophisticated model, which modifies the surface interplanar force constant only slightly, includes an additional surface stress term in the lattice dynamics. Such a model successfully explains the surface phonon dispersion results for Ni(100) [21,22], Ni(110) [23], and Ni(111) [24], and Cu(100) [25,26]. The magnitude of surface stress included in the lattice dynamics depends directly on the surface atomic density in the direction that the surface phonon mode propagates.

The main purpose of this paper is to test the extent to which FS potentials can be used to describe the dynamical properties of the three basal surfaces of Ni and Cu. The basis of this comparison will be to compare the calculated surface phonon spectral densities with the experimentally derived surface phonon dispersion relations for these surfaces. We have calculated the FS potential based surface phonon spectral densities for Ni and Cu using molecular dynamics simulations as described previously [30,31]. What makes FS potentials so valuable is that the surface bonding changes, i.e. the stiffening of the interplanar FC or the incorporation of an interplanar stress term, are automatically included in the form of the FS potential.

In the first section we describe briefly the FS potential model which was used and some of the computational details. The phonon density of states at various high symmetry points in the surface Brillouin zone (SBZ) are then presented

for the (100), (110), and (111) surfaces of Ni at 300 and Cu at 236 K. The first and second layer phonon spectral densities are presented so that modes localized to each layer can be compared to the experimentally measured dispersion curves obtained with HREELS and HAS. Since the only difference between the FS potentials for Ni and Cu are the scaling energy, ϵ, the calculated Ni spectral densities are also compared to experimental data on all three Cu faces. The layer-by-layer stress tensor terms and root-mean-square displacements (RMSD) have also been calculated during the simulations for comparison to the tensile stress terms in the lattice dynamics for Ni [21–24]. We summarize by discussing the differences between the FS and EAM derived model potentials, focussing on how these two potentials differ in their description of the attractive many-body binding potential.

2. Background

To first order, the binding energy of transition metals depends on the overlap character of the d-band orbitals [1]. The simplest expression relating the d-band orbitals to the total binding energy of the metal is the second-moment approximation to the tight-binding model, which states that the binding energy scales as the square root of the atomic coordination number [1,14]. This approximation relating the atomic coordination to the binding energy is especially good for Ni, Cu and other transition metals with mostly filled d-shells because the electron density from the d-orbitals can be spherically averaged, and higher order moments of the orbitals can be neglected [1].

The total energy per atom for a FS solid can be written as the sum of a repulsive pair-potential term and an attractive term proportional to the square root of the density [14],

$$E_i = \epsilon \left[\sum_{j \neq i} V(r_{ij}) - c\sqrt{\rho_i} \right], \tag{1}$$

where the atomic density, ρ_i, at the i-th site is a superposition calculated from the surrounding atomic density, $\psi(r_{ij})$. Sutton and Chen have chosen $V(r_{ij})$ and $\psi(r_{ij})$ to have $(a/r_{ij})^n$ functional forms, where a is the lattice constant for the FCC lattice, and have calculated the potential parameters for many transition metals [15].

During the MD simulations the atoms move according to Newton's equations of motion, $\boldsymbol{F} = m\boldsymbol{a}$. The force acting on the ith atom is given by [14],

$$\boldsymbol{F}_i = -\epsilon \left\{ \sum_{j \neq i} V'(r_{ij}) + c \sum_{j \neq i} \left[\left(\frac{1}{\sqrt{\rho_i}} + \frac{1}{\sqrt{\rho_j}} \right) \psi'(r_{ij}) \right] \right\} \frac{r_{ij}^{\alpha}}{r_{ij}}, \tag{2}$$

where the prime denotes differentiation with respect to r_{ij} and r_{ij}^{α} scales the calculated force in the α direction on the ith atom. The summation is over all j atoms where the interaction is significant and excludes the term when $i = j$. The details of the molecular dynamics simulation method and the equations necessary to carry out the simulations were previously discussed, including procedures for calculating surface phonon spectral densities [30,31].

To gain insight into the origin of the surface stress term used to describe the experimentally measured lattice dynamics, we have monitored the surface stress tensor during the simulations. The surface stress tensor is calculated using [32,33].

$$g_{\alpha\beta} = \frac{1}{2A} \sum_{j \neq i} \frac{F_i}{r_{ij}} r_{ij}^{\alpha} r_{ij}^{\beta}, \tag{3}$$

where A is the area of the surface and the units of the surface stress tensor are (N/m). This stress tensor term has the same units as a force constant, and is essentially the stress directed along the line of atoms parallel to the surface plane. The stress tensors for each layer were found by calculating the stress between the ith and jth atoms in each layer and adding these terms to the appropriate layers.

The Sutton and Chen potentials for Ni and Cu are identical except for the energy scaling factor ϵ and the lattice constant a. This seems reasonable considering that the measured dispersion curves for Cu and Ni, when scaled by their respective bulk maximum frequencies, appear

nearly identical [34]. In the simulations presented herein, we have used Ni potential parameters for all calculations. Cu results were derived by scaling the Ni results by the ratio $\epsilon_{Cu}/\epsilon_{Ni} = 0.788$. Because the lattice constant is scaled in the calculation of $V(r_{ij})$ and $\psi(r_{ij})$ in the $(a/r_{ij})^n$ functional form, using either the lattice constant for Ni or Cu will not make a difference in the dynamics. However, the simulation temperature chosen for the solid will be have to be scaled by $\epsilon_{Cu}/\epsilon_{Ni}$ to obtain the corresponding temperature for Cu. This can be understood by examining the melting point ratio of the two solids ($T^m_{Ni} = 1726$ and $T^m_{Cu} = 1358$ K) i.e. $T^m_{Cu}/T^m_{Ni} = 0.787$, which is very close to $\epsilon_{Cu}/\epsilon_{Ni}$. A more substantial argument is that through equipartition the kinetic energy (temperature) and dynamical potential energy are equal (this is discussed in detail in ref. [30]). Because the potential energy of the solid scales with ϵ, the temperatures will also scale with ϵ, or $\epsilon_{Cu}/\epsilon_{Ni}$ [30].

3. Simulation results

Before presenting the surface phonon spectral densities, root-mean-square displacements (RMSD), and stresses, we point out several trends in these measured quantities that are a direct consequence of using FS potentials. This is done so that the simulated results are easier to understand.

Because the force acting on each atom is scaled by the density term as $1/\sqrt{\rho_i}$, the net force acting on a particular atom will depend on its coordination, i.e., on which layer of the simulated solid it resides. Atoms with bulk coordination in all directions have a density weighting of the dynamics which is constant, and eq. (2) takes the form similar for F_i obtained when using pair-potentials [30,31]. However, near the surface, the atomic coordination changes abruptly between the first and second layer. Atoms in the first layer are scaled by a larger value of $1/\sqrt{\rho_i}$ and therefore will have a larger net force acting on them both in the surface plane and normal to it.

This increase in net force between the first and second layers will increase the Rayleigh wave frequency from what would be predicted from the bulk potential interaction, i.e. if the density term is not included in eq. (2). Another consequence is that the Rayleigh wave frequency will be closer to the bulk band edge and for some lower values of $\bar{Q}$ it may even be partially embedded in the bulk modes, depending on the surface force field that was used. Since the Rayleigh wave is located closer to or embedded in the bulk band edge, it will couple more strongly to the bulk modes, and a high energy tail can occur in the surface phonon spectral density.

The surface geometries and directions used in this study are shown in fig. 1. The atoms are $a/\sqrt{2}$ apart from each other, where a is the FCC lattice constant. This makes the $\hat{x}$ unit direction equal to $a/\sqrt{2}$. The $\hat{y}$ unit direction was chosen to be $\hat{y} = a/\sqrt{2}$ for the (100), $\hat{y} = a$ for the (110), and $\hat{y} = \sqrt{(3/2)}\,a$ for the (111). The $\hat{z}$ unit direction is chosen normal to the surface. For each different

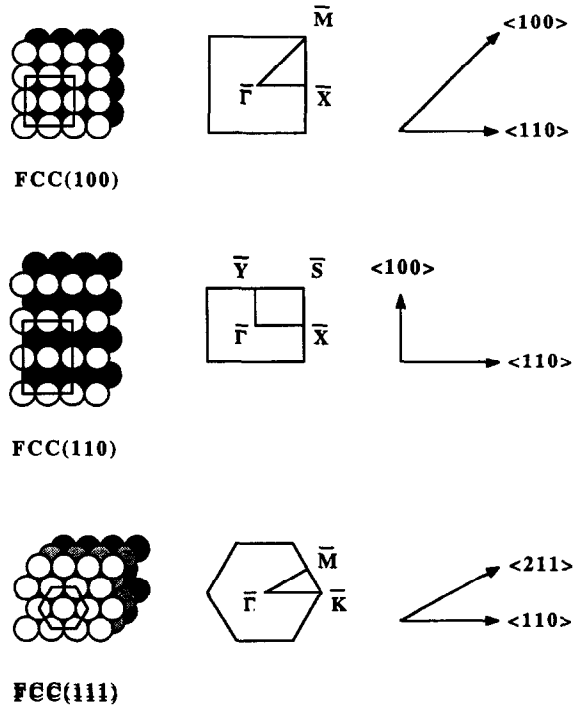

Fig. 1. Diagram of the (100), (110) and (111) surface planes. The left hand side panel has the real space geometric arrangement of the surface atoms, the middle panel has the two dimensional surface Brillouin zone, and the right hand side has the major symmetry directions.

temperature the thermal expansion of the lattice is accounted for by setting the lattice constant, $a = a_0 \exp[1.2 \times 10^{-5}(K^{-1})T]$, where a_0 is 3.52 Å and T is the temperature in K [35]. A total of 3100 atoms was used in each simulation, with a 10×10 array of atoms located on the top and bottom of a parallelpiped slab, which is surrounded by periodic boundary conditions [36].

The interactions were summed over the neighbor table twice for each time step [30], once to get the atomic density, and once to get the force for each direction, eq. (2). For this reason the maximum number of atoms that are included in these sums was set at 86. This corresponds to setting the cutoff radius at $r_c = (2.5/\sqrt{2})a$. The computational effort required for these calculations was nearly identical to simulations using Lennard-Jones potentials which included 176 in the neighbor table [30,31].

All simulations in this paper were conducted at $T = 300$ K for Ni. This corresponds to a simulation temperature of $T = 236$ K for Cu. No attempt was made to calculate the melting temperature for each material, but we note that simulations up to 700 K displayed no evidence of atoms moving out of their initially assigned lattice positions. The integration time step was 2.5 fs, which corresponds to about 100 time steps per maximum vibrational frequency (37.6 meV) for bulk Ni. With this time step, an energy resolution of 0.404 meV is achieved for 4096 time steps. The first and second layer spectral densities, $f^{\alpha\beta}(\bar{Q}; l_z, \omega)$, were obtained by adding the spectral densities from a total of 10 simulation runs. These runs were taken consecutively, with the final coordinates from the previous runs providing the initial coordinates for each successive run [30,31]. The spectral densities were measured once equilibrium was attained, $\alpha(\tau) = 5/3$, and surface temperatures were equal to 300 K [30,31].

4. Atomic displacements

The amount of interplanar relaxation that occurs can be calculated from the initial and final positions of the simulation. For all three basal surfaces the first-to-second layer interplanar distance decreases (the first layer relaxes inwards towards the bulk). This is shown in table 1 as a percent change of the bulk interplanar spacing. Our results agree well with the interlayer relaxations measured from various experimental techniques for Ni [37–40] and Cu [41–45].

Also listed in table 1 for comparison are the interplanar lattice relaxations which were obtained using EAM potentials [46]. Since the Ni and Cu FS potentials are identical except for an energy scaling factor, FS potentials give identical interlayer relaxations for both Ni and Cu. The Ni EAM derived surface relaxations agree exceptionally well with the Ni FS derived relaxations, but not as well with those for Cu [46]. In fact, the FS and EAM Ni relaxations agree better with each other than to the experimental values for first layer relaxations.

The RMSD were also measured for all three surfaces. A plot showing the three directional components as a function of layer number is shown in fig. 2. [Notice that the RMSD for the (110) surface are plotted with a slightly reduced y scale.] In this figure, layer 1 is the surface layer and layer 16 is the middle or bulk of the simulation slab. The 1st layer RMSD values are an average of the 1st layer and the 31st layer, the

Table 1
First and second interlayer relaxation for the three surfaces of Ni and Cu [a]

	Surface	FS(%)	EAM(%) [b]	Exp.(%)	Ref.
Ni	(100)	−2.9	−3.04	−3.2±0.5	[37]
	(110)	−7.1	−7.01	−8.7±0.5	[38]
				−9.0±1.0	[39]
	(111)	−1.9	−1.85	−1.2±1.2	[40]
Cu	(100)	−2.9	−3.79	−2.1±1.7	[41]
				−1.1±0.4	[42]
	(110)	−7.1	−8.73	−8.5±0.6	[43]
				−7.5±1.5	[44]
	(111)	−1.9	−2.48	−0.7±0.5	[42,45]

[a] The relaxations are listed as the fractional change in the interlayer spacing. The first column contains the results of the molecular dynamics simulation work in this paper. The second column lists the EAM derived relaxations [46], and the results from various experimental determinations.
[b] See ref. [46].

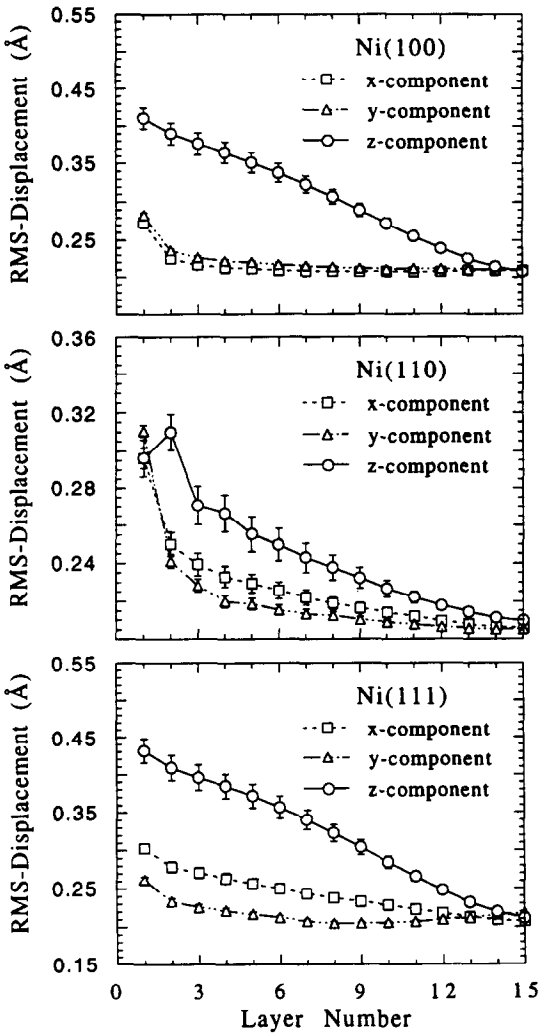

Fig. 2. The layer-by-layer root-mean-square displacements (RMSD) are plotted for all three directional components. Notice that the RMSD for the Ni(110) surface are plotted on a different scale. The RMSD appropriate for Cu can be obtained by scaling the Ni RMSD by 1.03.

2nd layer values are an average of the 2nd layer and the 30th layer, et cetera. On all three surfaces the $\hat{z}$-component of the RMSD has in general the largest value of the three components and decreases monotonically into the bulk of the material. However, this is not true for the first layer on the (110) surface, where the $\hat{y}$-component RMSD is larger. This $\hat{y}$-component direction corresponds to motions that vibrate perpendicularly to the rows of atoms on this surface. Similar increases in the y-component were also found on the (110) surface using Lennard-Jones potentials [30]. The reason why the (110) surface's $\hat{z}$-component RMSD is less than that for the second layer is a direct result of the stiffening of the force between the first and second layer atoms, as discussed previously. This increase in the second layer $\hat{z}$-component RMSD has also been observed using Ni EAM potentials [35].

4.1. (100) Surface

The Ni(100) surface phonon spectral densities were calculated for a simulation temperature of 300 K. The spectral densities at $\overline{X}$ for the surface layer (top panel) and for the second layer (bottom panel) are shown in fig. 3. In this figure, the $\hat{x}$-polarization is represented by the long-dashed line, the $\hat{y}$-polarization by the short-dashed line, and the $\hat{z}$-polarization by the solid line. The energy scale used in fig. 3 and for all subsequent spectral densities is appropriate for Ni. The energy scale for the phonon spectral density for Cu can be obtained from that of Ni by multiplying by $\epsilon_{Cu}/\epsilon_{Ni} = 0.7880$. For all modes discussed in this section, the mode assignment, polarization, the layer(s) in which the mode was observed, and the mode's energy are shown in table 2.

In fig. 3, a total of 3 surface modes and 3 surface resonances are observed in the first and second layer spectral densities. At $\overline{X}$, the S_1 mode occurs at 9.3 meV and is polarized in the $\hat{y}$-direction which corresponds to a shear horizontal (SH) motion of the surface atoms (orthogonal to the direction of propagation). The S_4 mode or Rayleigh wave is observed at 13.5 meV and has a z-polarization or shear vertical (SV) motion in the first layer. The S_4 mode also has a large $\hat{y}$-polarized and some $\hat{x}$-polarized intensity in the second layer. This large amount of second layer SH character of this mode is directly related to the crossover in this mode's first layer character from SV to SH between $\overline{X}$ and $\overline{M}$ [47]. The S_4 mode has a large high energy shoulder which is due to coupling between the surface Rayleigh wave and the bulk modes as discussed previously. The S_6 mode or longitudinal mode is observed at

25.1 meV and has predominantly $\hat{x}$-polarization in the first layer.

In addition to three surface modes, three surface resonances are observed predominantly in the second layer. The R_4 resonance which is $\hat{z}$-polarized and localized to the second layer is observed at 15.0 meV. We have labeled the resonance modes in this paper according to the experimental HREELS assignments of Rocca et al. [22]. The R_4 resonance has the same character as the S_5 mode reported by Allen et al. using Lennard-Jones potentials [47] except that it is mixed with the bulk modes and therefore is not a true surface mode. Another first and second layer z-polarized at 31.0 meV is the R_6 resonance. This resonance is "optical" in character and is similar to the S_8 mode [47]. It is shifted to a higher energy because of the increase in force between the first and second layers. The third resonance mode is the R_6 which occurs at 31.5 meV and is primarily x-polarized. At $\bar{X}$, the R_5 and R_6 modes overlap each other in energy but should separate in energy near $\bar{\Gamma}$ [22].

The first and second layer spectral densities at $\bar{M}$ are plotted in fig. 4. Two modes are observed, the S_1 at 17.8 and the S_2 at 20.5 meV. The S_1 is strictly localized to the surface layer while the S_2 has in-plane polarization ($\hat{x}$ and $\hat{y}$ polarization)

Table 2
Phonon energies obtained from the Ni MD simulations for various high symmetry points on all three surfaces [a]

Miller index	$\bar{Q}$	Pol. $(\hat{x},\hat{y},\hat{z})$	Layer (1,2)	Mode assign	FS energy (meV)	Measured (meV)	Difference (meV)
(100)	$\bar{X}$	y	1	S_1	9.3 (1.6)	not obs.	–
		z	1	S_4	13.5 (1.0)	16.3 ± 0.5	2.8
		x	1	S_6	25.1 (2.2)	31.1 ± 0.3	6.0
		z	2	R_4	15.0 (2.3)	18.7 ± 0.7	4.0
		z	2	R_5	31.0 (2.5)	33.5 ± 0.5	2.5
		x	2	R_6	31.5 (2.5)	33.5 ± 0.5	2.0
	$\bar{M}$	z	1	S_1	17.9 (1.2)	19.3 ± 0.6	1.4
		z	2	S_2	20.6 (0.8)	25.4 ± 0.4	4.9
(110)	$\bar{X}$	z	1	S_1	13.5 (1.4)	17.1 ± 0.5	3.6
		y	1	S_2	16.3 (1.2)	20.9 ± 1.0 [b]	4.6
		x	1	S_7	23.8 (2.2)	28.0 + 1.0 [b]	4.2
		y	2	R_1	22.0 (1.8)	25.0 ± 1.0 [b]	3.0
		x	2	R_2	31.0 (4.3)	34.6 ± 1.0 [b]	3.6
	$\bar{Y}$	y,z	1,2	S_1	8.0 (1.1)	10.0 ± 0.4	2.0
		x	1	S_2	10.9 (1.6)	14.4 ± 1.0 [b]	3.5
		z	1	S_3	12.5 (1.3)	15.4 ± 0.4	2.9
		y,z	1,2	S_5	20.2 (1.3)	not obs.	–
		y	2	R_2	32.0 (1.5)	33.8 ± 0.5	1.8
(111)	$\bar{M}$	z	1,2	S_1	13.3 (0.8)	17.2 ± 0.2	3.9
		y	1,2	PRW	14.1 (1.0)	not obs.	–
		x	1	S_2	27.1 (2.4)	32.2 ± 0.2	5.1
		z	2	R_1	20.9 (1.7)	23.1 ± 0.2	2.2
		x	2	R_2	31.6 (3.0)	not obs.	–

[a] The first two columns list the surface and the corresponding high symmetry point. The third column lists the main polarizations and the fourth column lists the layer or layers where the mode is observed. The fifth column lists the mode assignment following the nomenclature of Allen, Alldredge, and de Wette [47]. In the sixth column the phonon energy associated with each of these modes is listed. If it was observable, the seventh column contains the experimentally measured phonon energy for each mode: Ni(100) [21,22], Ni(110) [23a,b] and Ni(111) [24]. The last column gives the difference between the experimentally measured energy and the FS simulation results.

[b] See ref. [23b].

in the first layer. Two resonance modes are also observed in the spectral densities, the R_1 at 21.5 meV with SV polarization and the R_2 which reaches a maximum at 32 meV with in-plane polarization. The MD calculated phonon spectral density intensities agree very well with the spectral intensities calculated using the slab technique by Rocca et al. for Ni(100) [22].

We now compare the results from the MD simulation to the experimentally measured dispersion curves (both HREELS [21,22] and HAS

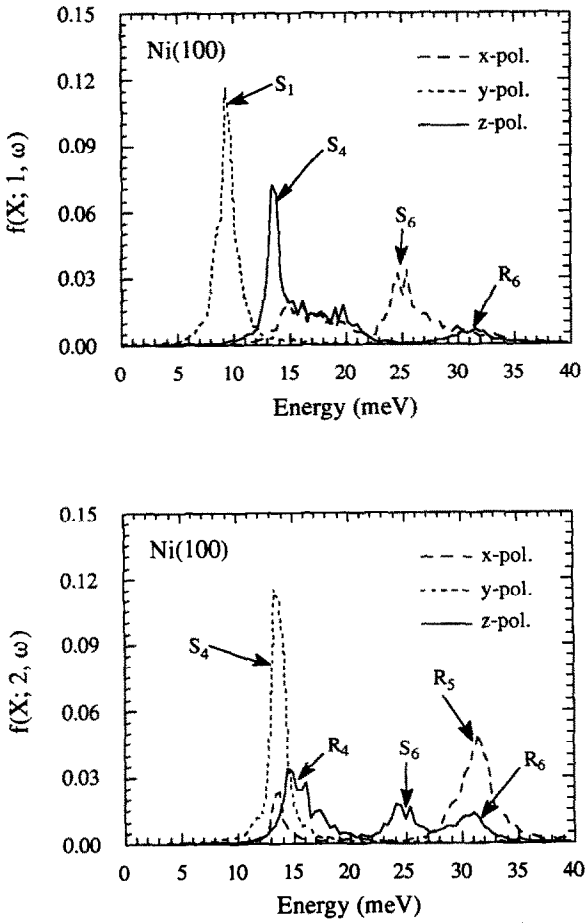

Fig. 3. First (top panel) and second (bottom panel) layer phonon spectral densities for Ni(100) at $\bar{X}$. The $\hat{x}$-polarized spectral density is plotted by a dashed line, the $\hat{y}$-polarized modes by a dot-dashed line, and the $\hat{z}$-polarized modes by a solid line. The energies for the Cu(100) at $\bar{X}$ can be obtained by dividing the Ni phonon energy by 1.269.

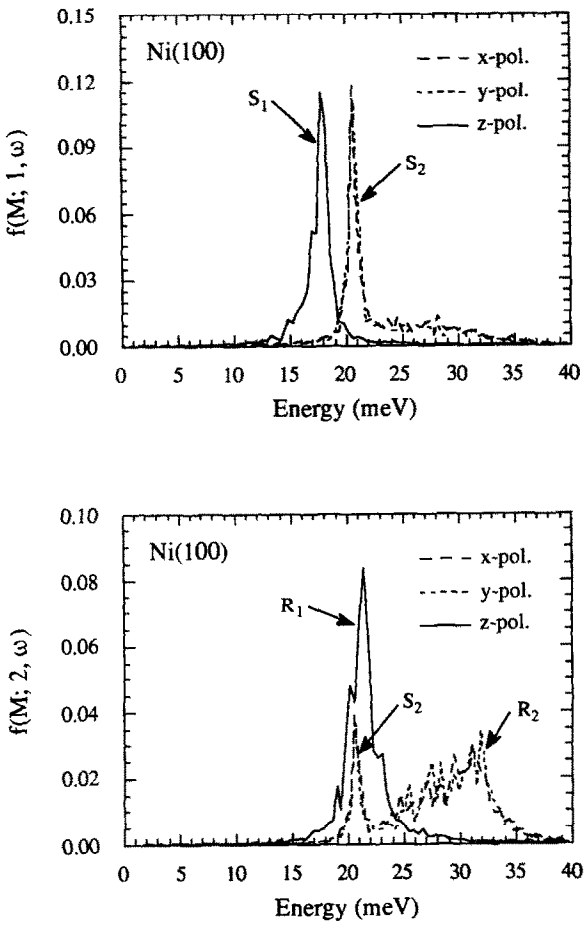

Fig. 4. Same as fig. 3, except the spectral densities are for Ni(100) surface at $\bar{M}$.

[48]) on Ni(100). Early HREELS experiments resolved only one mode near $\bar{X}$ at 16.4 meV [21]. However, additional modes were later found at 19.0, 31.1, and 33.6 meV [22]. HAS measurements have confirmed that the Rayleigh wave frequency is 16.4 meV at $\bar{X}$ [48]. HAS measurements also observed a longitudinal mode out to 80% of the SBZ along the $\bar{\Gamma}$–$\bar{X}$ direction. HREELS data at $\bar{M}$ display two modes, the S_1 at 19.2 meV and the S_2 mode at 25.8 meV [22]. Each of the frequencies of the experimentally observed modes are listed in table 2 next to the frequency from the simulation. The R_4, R_5, and R_6 modes are also observed at $\bar{X}$ and the R_1 at

$\overline{M}$ is not totally resolved from the S_2. The energies, polarizations, and localizations are shown in table 2.

For the (100) surface, each of the MD obtained mode frequencies listed in table 2 is lower than the experimentally observed values. This deviation is largest for the first layer in-plane modes, especially the S_6 at $\overline{X}$ and the S_2 at $\overline{M}$. Better agreement is attained for the vibrations normal to the surface plane ($\hat{z}$-polarized modes) and modes localized in the second layer. The reason why the in-plane first layer modes deviate more is because the density (i.e. the number of nearest neighbors) is less for both surface atoms, i.e., the calculated in-plane force constant [eq. (2)] is scaled by $1/\sqrt{\rho_i}$ for both atoms. For vibrations located in the second layer, or for out-of-plane displacements, the force component for only one of the atoms is scaled by the density term. (These results are not surprising since the FS formulation underestimates the surface electronic density.) All of the vibrational modes which have been measured experimentally have some $\hat{z}$-component motion in either the first or second layer [21,22,48].

When the simulated phonon frequencies are scaled by $\epsilon_{Cu}/\epsilon_{Ni} = 0.7880$ we obtain the Cu(100) frequencies. These are compiled in table 3 and are also lower than the experimentally measured phonon frequencies for Cu(100) [25,26]. The experimental phonon frequencies and the MD results for the S_4 at $\overline{X}$ and the S_1 at $\overline{M}$ are shown in table 3. Both of these modes are the $\hat{z}$-polarized modes (i.e. the Rayleigh wave) and the difference between the experimental and the MD simulated results is identical.

4.2. (110) Surface

The number of modes localized to the surface on the (110) surface is larger than on either the (100) or the (111) [47]. Because of its lower surface coordination, the majority of intense surface phonon modes on the (110) surface are shifted to lower energies than on the (100) or the (111) surfaces. The dynamical behavior of metal (110) surfaces have recently attracted considerable attention in connection to surface roughening [20,49–55] and anharmonic effects [20,49–51]. For example, recent results indicate that the decrease in specular intensity of the surface reflected beams near half of the melting point of the material is more likely to be due to anharmonic potential terms than to surface roughening. This increased anharmonicity has been demonstrated in recent HAS experiments [49], where no increase in the number of steps is observed and in MD simulation using the EAM and EMT potentials [10,35]. A study of the temperature dependence of Ni(110) using Finnis–Sinclair potentials will be the subject of a future paper [56].

Table 3
Same as table 2 except the FS energies have been scaled for Cu: Cu(100) [25,26], Cu(110) [27,28], and Cu(111) [19,29]

Miller index	$\overline{Q}$	Pol. $(\hat{x},\hat{y},\hat{z})$	Layer(1,2)	Mode assign	FS energy (meV)	Measured (meV)	Difference (meV)
(100)	$\overline{X}$	z	1	S_4	10.6 (0.8)	13.4 ± 0.2	2.8
	$\overline{M}$	z	1	S_1	14.1 (0.9)	16.6 ± 0.3	2.5
(110)	$\overline{X}$	x	1	S_7	18.8 (3.0)	23.9 ± 0.2	5.1
	$\overline{Y}$	y,z	1,2	S_1	6.0 (1.0)	7.0 ± 0.2	1.0
		z	1	S_3	9.9 (1.0)	12.1 ± 0.2	2.2
		y,z	1,2	R_2	21.1 (4.0)	23.1 ± 0.2	2.0
(111)	$\overline{M}$	z	1,2	S_1	10.5 (0.6)	13.0 ± 0.2	2.5
		z	2	R_1	16.5 (1.3)	18.3 ± 0.6	1.8
		x	1	S_2	21.4 (1.9)	25.5 ± 0.2	4.1
		x	2	R_2	24.9 (2.4)	28.3 ± 0.2	3.4

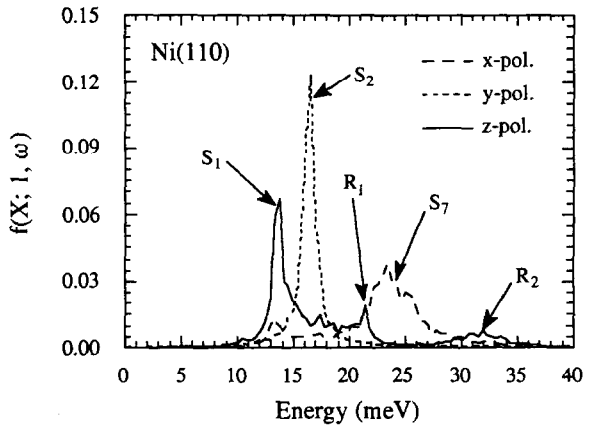

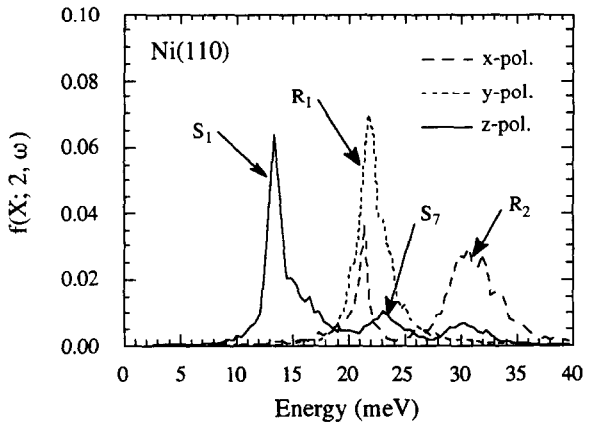

Fig. 5. Same as fig. 3, except the spectral densities are for Ni(110) surface at $\overline{X}$.

The modes for the first and second layers at $\overline{X}$ are plotted in fig. 5. Three modes that have a large intensity in the first layer are observed at 13.5, 16.3, and 23.8 meV. The $\hat{z}$-polarized mode at 13.5 meV is the S_1 mode (Rayleigh wave); this mode also has a large intensity in the second layer. The first layer $\hat{z}$-polarized spectral density (above 13.5 meV) also contains a large amount of bulk intensity, indicating that the surface Rayleigh mode is coupled to the surface projected bulk bands. The peak at 16.3 meV is the S_2 mode. It has SH polarization ($\hat{y}$-component), and is not observed for in-plane HAS or HREELS scattering. The peak at 23.8 meV is the S_7 mode, and has SV in-plane motion in the first layer and small component of surface normal motion in the second layer. The S_7 mode has a large energy linewidth, which is due to its strong coupling to the R_1 resonance mode in the second layer at 22 meV. The other surface resonance mode, the R_2, at 31 meV has a small $\hat{z}$-polarized intensity in the first layer and a large $\hat{x}$-polarized intensity in the second layer.

For atomic motion propagating perpendicularly to the atomic rows at $\overline{Y}$, three distinct surface modes are observed below the bulk band and are shown in fig. 6. These are the S_1 at 8.0, the S_2 at 10.9, and the S_3 at 12.5 meV. Of these modes, two are experimentally observable, the S_1 which has a SV component in both the first and

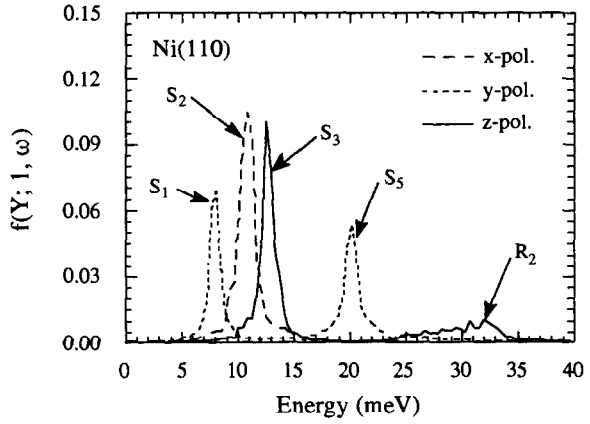

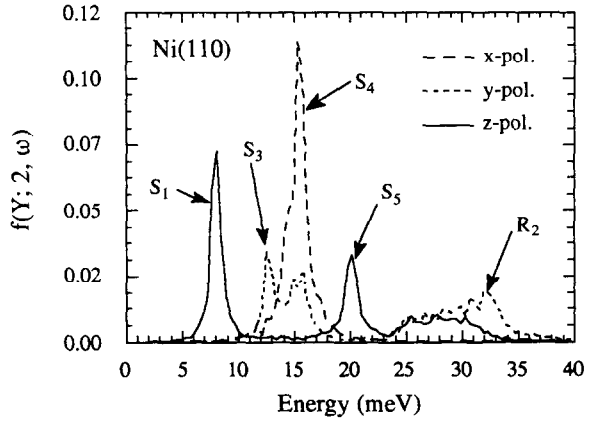

Fig. 6. Same as fig. 3, except the spectral densities are for Ni(110) surface at $\overline{Y}$.

second layer, and S_3 which is the Rayleigh wave (at $\overline{Y}$ the $\hat{y}$-component of motion is SV polarized and the $\hat{x}$-component of motion is SH polarized). The S_5 is also observed at 20.2 meV in the band gap at $\overline{Y}$. In the second layer the S_4 occurs at 15.2 meV and has SH polarization. Some $\hat{y}$ and $\hat{z}$-component intensity is also observed in the 25–34 meV energy range which is due to the R_2 surface resonance [23]. As for the case of Ni(100), the calculated phonon spectral density intensities agree well with the force constant model developed to explain the experimental HREELS data for Ni(110) [23].

The experimentally determined phonon frequencies for Ni(110) and Cu(110) are shown in tables 2 [23] and 3 [27,28], respectively. On Ni(110), recent HREELS measurements reveal 5 modes at $\overline{X}$, the S_1, S_2, S_7, R_1 and R_2. All 5 modes are observed in the calculated spectral densities shown in fig. 5. To explain these experimentally measured phonon frequencies non-central forces were introduced [23b], along with slight modifications of the earlier force constant model used to explain the earlier measurements [23a]. These non-central forces are automatically included in the FS model potential. As observed on the (100) surface the experimentally measured phonon frequencies are systematically larger than in the simulation. The reason for this will be addressed in the discussion section of this paper.

4.3. (111) Surface

This surface has the least complicated surface phonon spectrum because it has the fewest number of distinct surface modes [47]. The MD calculated surface and second layer phonon spectral densities at $\overline{M}$ are plotted in fig. 7. The S_1 mode occurs at 13.3 meV with $\hat{z}$-polarization in both layers, and couples strongly to the surface projected bulk modes at higher frequencies. This increased density of bulk modes at the surface is largest for the (111) surface and least on the (110). The reason for this is that the Rayleigh wave is closer to the bulk band edge on the (111) than the (110) surface. The S_2 mode is observed at 27.1 meV with $\hat{x}$-polarization on the first layer. A third mode with a strong SH polarization is observed at 14.1 meV in both layers. This mode is

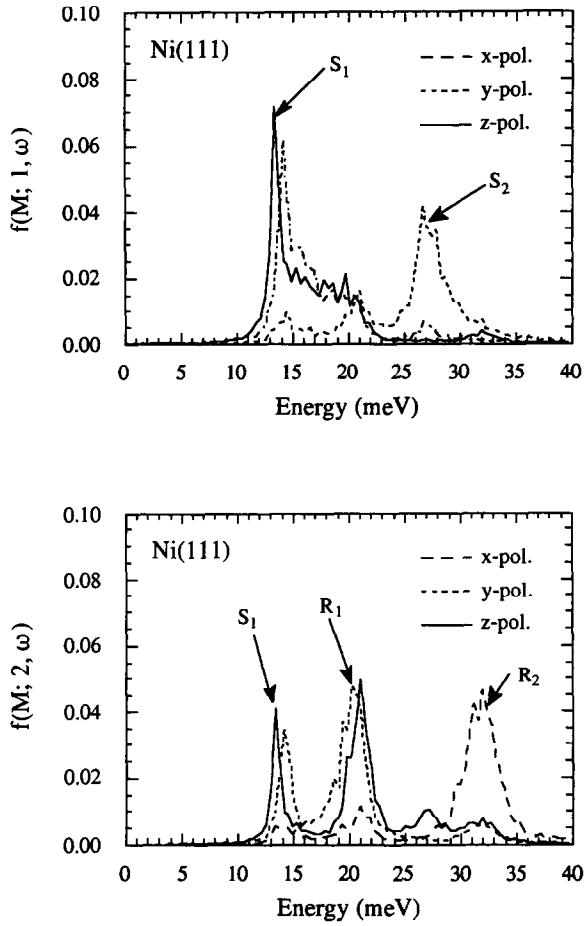

Fig. 7. Same as fig. 3, except the spectral densities are for Ni(111) surface at $\overline{M}$.

likely the "pseudo" Rayleigh wave observed in HAS experiments on Pt(111) [57], but not resolved on the Ni(111) surface [24]. Two surface resonances are observed in the second layer, the R_1 at 20.9 meV with strong z-polarization and the other, the R_2 at 31.6 meV with $\hat{x}$-polarization.

Three modes at $\overline{M}$ were observed by Menezes et al., at 17.2 (S_1), 32.2 (S_2), and 23.1 (SR = R_1) meV [24], and are listed in table 2. The experimentally measured HAS [29] and HREELS [19] phonon frequencies for Cu(111) are listed in table 3. The HREELS does reveal the two surface modes, the S_1 and S_2, and also the two resonance modes, the R_1 and R_2. Similar to the (100) surface, better agreement between the experimental

frequencies and the simulated phonon frequencies is obtained for the $\hat{z}$-polarized first and second layer modes than the in-plane modes in the second layer (i.e. resonance modes).

4.4. Surface stress

Surface atoms do not necessarily sit at the minimum of their in-plane potential energy since they may be more tightly held by the corrugated potential established by the bulk lattice [32,33]. This introduces a lateral stress on the atoms in the surface plane, which when multiplied by the atomic separation applies an additional force on the atom. Addition of a surface stress term has been recently used to explain the lattice dynamics of the three basal faces of Ni [22–24] and the Cu(100) surface [26]. For this reason the surface stress terms were calculated during the simulations using eq. (3).

For all three surfaces the surface stress was negative with the largest component of stress found in the in-plane directions ($\hat{x}\hat{x}$ and $\hat{y}\hat{y}$ tensors). Negative values for the stress tensor correspond to a tensile stress (attractive interaction between atoms) while positive values for the stress tensor correspond to a compressive stress (repulsive interaction between atoms). Atoms subjected to a tensile stress would expand away from a surface vacancy if one was created on the surface. Because of symmetry the $\hat{x}\hat{x}$ and $\hat{y}\hat{y}$ components of the surface stress tensor are identical on the (100) and (111) surface but on the (110) surface they are not. The negative values for the first three layers of the layer-by-layer stress tensor are listed in table 4 for Ni, along with the theoretical values used in the lattice dynamics to match to the experimental HREELS surface phonon dispersion measurements [21–24].

The largest calculated intraplanar stress was found for the (100) surface and lowest on the (110) surface. This progression is different from the stress terms used to explain the experimentally measured HREELS phonon data on the three faces of Ni listed in table 4; Ni(100) [21,22], Ni(110) [23], and Ni(111) [24]. Good agreement is found between the simulation results for the intraplanar stress and the experimental values for the (100) and (111) surfaces. The experimentally derived intraplanar stresses are slightly larger than the simulated intraplanar stresses. This is a consequence of the potential model used and is explained in the following section. However, there is a large difference between the MD simulated stress and the surface stress terms used to explain the dynamics for Ni(110) [23]. This discrepancy for the (110) surface is due to the fact that the experimentally obtained stress was assumed to reside only on the surface layer, while the calculated stresses shown in table 4 appear to extend significantly down to the third layer. This gradual change in the stress tensors near the surface on the (110) may be physically more realistic because it would correspond more closely to the gradual change in the atomic density or coordination from the surface to the bulk. This correspondence between the atomic density and the magnitude of surfaces stress has been tabulated by Menezes et al. [24].

Table 4
Results of the molecular dynamics measured stress calculated from eq. (3) [a]

Miller index	Finnis–Sinclair $-\phi'/r$ (N/m)				Ex. work
	1st layer	2nd layer	3rd layer	bulk	
(111)	1.357	−0.230	−0.232	−0.225	1.6±0.2
(100)	1.633	−0.027	−0.069	−0.050	1.9
(110)⟨1$\bar{1}$0⟩	1.209	0.052	−0.112	−0.147	3.0±1.5
(110)⟨100⟩	0.918	0.220	−0.034	−0.077	4.2±1.8

[a] The layer-by-layer stress is listed for the first three surface layers and the bulk layer. The last column lists the stress obtained from force constant model fits to the experimentally obtained surface phonon data, which have been compiled in Menezes et al. [24].

5. Discussion

In this paper we have calculated the phonon spectral densities on the fcc (100), (110) and (111) surfaces of Ni and Cu using molecular dynamics simulations. We have used the Finnis–Sinclair potentials suitable for Ni and Cu to model the dynamical properties of these metal surfaces. The simulation temperature was set to 300 K for Ni so that the simulated phonon spectral densities could be compared to the experimentally measured sur-

face phonon dispersion relations for Ni and Cu. No attempt was made to modify the FS potential model parameters to better match the surface phonon frequencies. The reason for this is that the potential parameters were fit to bulk properties of Ni and Cu with the aim of describing the other properties of the solid, including for example the surface phonon spectral densities.

We found good overall qualitative agreement between the experimentally measured and simulated surface phonon frequencies. The calculated surface phonon spectral densities agreed well with the spectral densities obtained from the force constant fit to the experimentally measured phonon dispersion [19,22,23]. Good agreement was also obtained in the number of observable modes and their vibrational characteristics. On all three surfaces the simulated frequencies were always slightly lower than the corresponding experimental values.

The reason that the simulated surface phonon frequencies are lower than the experimental values is due in part to how the model potential parameters were chosen. The four potential parameters used in the simulation were fit by Sutton and Chen to the lattice energy and lattice constant for both Ni and Cu [15]. The values of the potential exponents, m and n, are chosen using the constraint that $m < n$. Once the values for m and n are chosen, the values of the well depth, ϵ, and the attractive potential scaling factor, c, are essentially fixed. The values of the parameters were chosen to match as closely as possible the bulk modulus, bulk vacancy formation, and the elastic constants, c_{11}, c_{12}, and c_{44}. Although this procedure produces a potential model that can be used to calculate many bulk, surface, and thermodynamic quantities, exact agreement between the theoretically obtained quantities and the experimentally measured quantities is generally not attained [15]. There is no a priori reason to expect that potentials derived from bulk elastic constants will quantitatively describe the vibrational spectrum at the surface.

The overall agreement of the model potentials in phonon frequency seems best for the (110) and (100) surfaces. This seems contradictory considering that the fact that the density term in eq. (2) is largest for the (110) surface (7 nearest neighbors) and the smallest for the (111) surface (9 nearest neighbors). It might be expected that this density term would change the dynamics of the (110) surface more than the (111) surface, so that the overall agreement between the model and the measured surface vibrations on a (111) surface might be better than the overall agreement of the surface vibrations on a (110) surface. However the opposite is true.

The reason why better overall agreement is obtained for the (100) and (110) surfaces, rather than for the (111), is that the density term's influence, i.e. the many-body binding term, on the dynamics at the surface is underestimated. If the may body binding potentials (i.e. $-c\sqrt{\rho_i}$) for the EAM and FS potential models are compared the FS many body binding term is always larger than that for the EAM, as shown in fig. 8. This leads to a corresponding underestimation in the value of $1/\sqrt{\rho_i}$ used in eq. (2) [2,3]. Also plotted in the bottom panel of fig. 8 are the derivatives of these potentials [2,3]. The derivative term is closely related to the calculated force used in the simulations since it appears in eq. (2). The surface atomic densities for the (100), (110), and (111) surfaces are shown as arrows in this figure. Near these surface atomic densities the EAM potential clearly has greater slope than the FS potential [2,3]. If the FS potential had a slightly greater slope near the (110) atomic density and a much larger slope near the (111) atomic density, better agreement might be attained between the calculated and experimental phonon dispersion curves. The origin of this underestimated is due to not considering higher order changes to the d-band near the surface, something which the EAM potentials address. To correct this deficiency in the FS model potentials, higher order terms could be added to the many body potential to account for second-order changes in the d-band structure.

The stress terms calculated during the simulation agree well with the experimentally determined stress terms for the (100) and (111) surfaces, but are systematically lower than the values derived from experiment [22–24]. The reason for

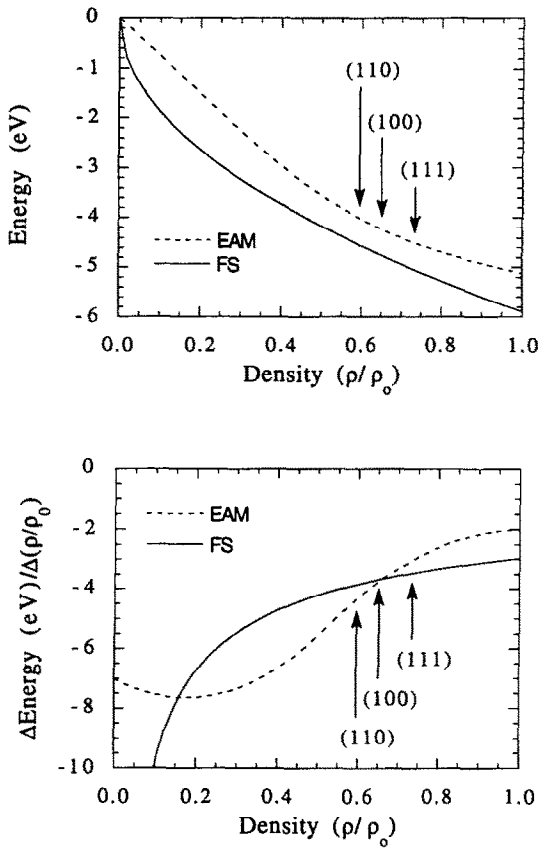

Fig. 8. Comparison of the FS and EAM many-body binding potentials as a function of the atomic density scaled to the bulk atomic density. The top panel shows both of the potentials and the bottom panel shows the derivative of the potentials. Arrows indicate the surface atomic density for each of the three basal surfaces.

this is again the decreased value of ψ' as explained in the previous paragraph.

Good agreement exists between the experimentally derived and MD calculated surface interplanar relaxations. Even better agreement is obtained between the EAM derived interplanar relaxations and the MD simulation results. All FS potential derived relaxations for all surfaces are less than those calculated with EAM potentials [46]. The relaxations agree best for the (110) surface, and are worst for the (111), for both Ni and Cu. This again implies that the scaled density term in eq. (2) should be increased.

6. Conclusion

In summary, we have used MD simulations to calculate the surface phonon spectral densities for the (100), (110), and (111) surfaces of Ni and Cu using Finnis–Sinclair (FS) model potentials. The phonon frequencies obtained from the FS model potentials were found to be systematically lower than the experimental values on all three surfaces of both metals. The reason for this is that the FS potential underestimates the influence of the many body binding potential. This underestimation is partially due to not explicitly calculating second-order changes in the d-band structure as is done in EAM methods. However, the Finnis–Sinclair potential model does qualitatively model the changes and trends in bonding at the surfaces of these metal. This is clearly seen when the surface phonon spectral densities obtained from MD simulations are compared with those derived from simple force constant models (i.e., lattice dynamics calculations) which reproduce the relevant experimental dispersion curves. First-to-second layer geometric separations calculated with FS and EAM potentials agree well with each other, better than when either set of results is compared to experimental values. The FS potentials certainly model the metallic surface vibrational characteristics and near surface structural relaxations better than those derived from Lennard-Jones potentials, which predict a first-to-second layer expansion and would shift the surface phonon frequencies even lower as compared to the bulk band edge.

When deriving model potential systems, what is typically desired is an atomic potential that can effectively model all physical properties of the material. In this paper we have shown that FS potentials derived exclusively from bulk properties provide a reasonably good description of the surface force field for the basal surfaces of Ni and Cu. To match the surface phonon dispersion energies even more closely a more detailed potential model must be developed. This would perhaps involve ab initio electronic structure calculations to derive more accurate near-surface potentials which could then be used in further MD studies of interfacial properties. We hope

that the comparisons we have provided in this paper will aid the further development of model potentials suitable for quantitative and efficient simulation of metal surfaces.

Acknowledgements

We would like to thank P. Knipp and D. Padowitz for helping with program development. This work was supported, in part, by the Air Force Office of Scientific Research and the National Science Foundation Materials Research Laboratory at the University of Chicago.

References

[1] A.E. Carlsson, in: Solid State Physics, Eds. H. Ehrenreich and D. Turnbull (Academic Press, New York, 1990) p. 1.
[2] M.S. Daw and M.I. Baskes, Phys. Rev. B 29 (1984) 6443.
[3] M.S. Daw and R.D. Hatcher, Solid State Commun. 56 (1985) 697.
[4] S.M. Foiles, M.I. Baskes and M.S. Daw, Phys. Rev. B 33 (1986) 7983.
[5] J.S. Nelson, E.C. Sowa and M.S. Daw, Phys. Rev. Lett. 61 (1988) 1977.
[6] J.S. Nelson, M.S. Daw and E.C. Sowa, Phys. Rev. B 40 (1989) 1465.
[7] P. Stoltze, J.K. Nørskov and U. Landman, Phys. Rev. Lett. 61 (1988) 440.
[8] P.D. Ditlevsen and J.K. Nørskov, J. Electron Spectrosc. Relat. Phenom. 54/55 (1990) 237.
[9] P.D. Ditlevsen and J.K. Nørskov, Surf. Sci., to be published.
[10] P.D. Ditlevsen, P. Stoltze and J.K. Nørskov, Phys. Rev. B 44 (1991) 13002.
[11] F. Ercolessi, M. Parrinello and E. Tosatti, Surf. Sci. 177 (1986) 314.
[12] F. Ercolessi, M. Parrinello and E. Tosatti, Philos. Mag. A 58 (1988) 213.
[13] X. Wang, Phys. Rev. Lett. 67 (1991) 1294.
[14] M.W. Finnis and J.E. Sinclair, Philos. Mag. A 50 (1984) 45.
[15] A.P. Sutton and J. Chen, Philos. Mag. Lett. 61 (1990) 139.
[16] L. Ningsheng, X. Wenlan and S.C. Shen, Solid State Commun. 67 (1988) 837.
[17] N. Luo, W. Xu and S. Shen, Phys. Status Solidi B 158 (1990) 493.
[18] R.B. Doak, U. Harten and J.P. Toennies, Phys. Rev. Lett. 51 (1983) 578.
[19] B.M. Hall, D.L. Mills, M.H. Mohamed and L.L. Kesmodel, Phys. Rev. B 38 (1988) 5856.
[20] A.P. Baddorf and E.W. Plummer, Phys. Rev. Lett. 66 (1991) 2770.
[21] S. Lehwald, J.M. Szeftel, H. Ibach, T.S. Rahman and D.L. Mills, Phys. Rev. Lett. 50 (1983) 518.
[22] M. Rocca, S. Lehwald, H. Ibach and T.S. Rahman, Surf. Sci. 171 (1986) 632.
[23] (a) S. Lehwald, F. Wolf, H. Ibach, B.M. Hall and D.L. Mills, Surf. Sci. 192 (1987) 131;
(b) M. Balden, S. Lehwald, H. Ibach, A. Ormeci and D.L. Mills, Phys. Rev. B 46 (1992) 4172.
[24] W. Menezes, P. Knipp, G. Tisdale and S.J. Sibener, Phy. Rev. B 41 (1990) 5648.
[25] M. Wuttig, R. Franchy and H. Ibach, Solid State Commun. 57 (1986) 445.
[26] M. Wuttig, R. Franchy and H. Ibach, Z. Phys. B Condensed Mater. 65 (1986) 71.
[27] B.F. Manson, K. McGreer and B.R. Williams, Surf. Sci. 130 (1983) 282.
[28] J.A. Stroscio, M. Persson, S.R. Bare and W. Ho, Phys. Rev. Lett. 54 (1985) 1428.
[29] U. Harten, J.P. Toennies and C. Wöll, Faraday Discuss. Chem. Soc. 80 (1985) 137.
[30] D.D. Koleske and S.J. Sibener, Surf. Sci. 268 (1992) 406.
[31] D.D. Koleske and S.J. Sibener, Surf. Sci. 268 (1992) 418.
[32] R.J. Needs, Phys. Rev. Lett. 58 (1987) 53.
[33] P.D. Ditlevsen, Thesis, Technical University of Denmark, Kopenhagen, 1991.
[34] D.D. Koleske, Thesis, University of Chicago, Chicago, 1992.
[35] E.T. Chen, R.N. Barnett and U. Landman, Phys. Rev. B 41 (1990) 439.
[36] W. Schommers, in: Structure and Dynamics of Surfaces I, Eds. W. Schommers and P. von Blackenhagen (Springer, Berlin, 1986) p. 199.
[37] J.W.M. Frenken, J.F. van der Veen and G. Allan, Phys. Rev. Lett. 51 (1983) 1876.
[38] D.L. Adams, L.E. Petersen and C.S. Sorensen, J. Phys. C 18 (1985) 1753.
[39] S.M. Talisove, W.R. Graham, E.D. Adams, M. Copel and T. Gustafsson, Surf. Sci. 171 (1986) 400.
[40] J.E. Demuth, P.M. Marcus and D.W. Jepsen, Phys. Rev. B 11 (1975) 1460.
[41] R. Mayer, C. Zhang, K.G. Kynn, W.E. Frieze, F. Jona and P.M. Marcus, Phys. Rev. B 35 (1987) 3102.
[42] H.L. Davis and J.R. Noonan, Surf. Sci. 126 (1983) 245.
[43] D.L. Adams, H.B. Nielsen, J.N. Andersen, I. Stensgaard, R. Feidenhansl and J.E. Sorense, Phys. Rev. Lett. 49 (1982) 669.
[44] M. Copel, T. Gustafsson, E.T. Graham and S.M. Yalisove, Phys. Rev. B 33 (1986) 8110.
[45] S.A. Lindgren, L. Walldén, P. Anderson and P. Westrin, Phys. Rev. B 29 (1984) 576.
[46] N. Ting, Y. Qingliang and Y. Yiying, Surf. Sci. 206 (1988) L857.
[47] R.E. Allen, G.P. Alldredge and F.W. de Wette, Phys. Rev. B 4 (1971) 1661.
[48] R. Berndt, J.P. Toennies and C. Wöll, J. Electron Spectrosc. Relat. Phenom. 44 (1987) 183.

[49] P. Zeppenfeld, K. Kern, R. David and G. Comsa, Phys. Rev. Lett. 62 (1989) 63.
[50] H. Dürr, R. Schneider and T. Fauster, Phys. Rev. B 43 (1991) 12187.
[51] A.P. Baddorf and E.W. Plummer, J. Electron Spectrosc. Relat. Phenom. 54/55 (1990) 541.
[52] S.G.J. Mochrie, Phys. Rev. Lett. 59 (1987) 304.
[53] G.A. Held, J.L. Jordan-Sweet, P.M. Horn, A. Mak and R.J. Birgeneau, Phys. Rev. Lett. 59 (1987) 2075.
[54] J.W.M. Frenken, R.J. Hamers and J.E. Demuth, J. Vac. Sci. Technol. A 8 (1990) 293.
[55] Y. Cao and E.H. Conrad, Phys. Rev. Lett. 64 (1990) 447.
[56] D.D. Koleske and S.J. Sibener, Surf. Sci., to be published.
[57] V. Bortolani, A. Franchini, G. Santoro, J.P. Toennies, C. Wöll and G. Zhang, Phys. Rev. B 40 (1989) 3524.